Carbohydrate Polymers 225 (2019) 115248

Contents lists available at ScienceDirect

Carbohydrate Polymers

journal homepage: www.elsevier.com/locate/carbpol

Polyethyleneimine-crosslinked cellulose aerogel for combustion CO_2 capture

Cheng Wang[a], Satoko Okubayashi[a,b,*]

[a] Advanced Fibro-Science, Kyoto Institute of Technology, Kyoto, 606-8585, Japan
[b] Research Institute for Sustainable Humanosphere, Kyoto University, Kyoto, 611-0011, Japan

ARTICLE INFO

Keywords:
3D structure
Nanoscale pore
Solid adsorption materials
CO_2 adsorption
Adsorption kinetic

ABSTRACT

Polyethylenimine (PEI) will block the channel of pore when it was impregnated in the porous solid, limiting its practical application in CO_2 adsorption. In this method, a novel polyethyleneimine-crosslinked cellulose (PCC) aerogel sorbent was prepared by the sol-gel process, hydrolysis reaction and crosslinking reaction. The specific surface area of porous PCC aerogel was still retained 234.2 m^2/g when the content of nitrogen was 17.4 wt%. The CO_2 adsorption capacity of PCC aerogel reached 2.31 mmol/g at 25 °C under pure dry CO_2 atmosphere. Pseudo-second order model perfectly is suitable to predict the CO_2 adsorption behaviors of PCC aerogel at different temperatures. The CO_2 diffusion mechanism of PCC aerogel was limited by not only intra-particle diffusion but also surface diffusion. The PCC aerogel showed excellent CO_2 adsorption-desorption recyclability after 10 cycles. This work proved that the PCC aerogel played an important role as a potential CO_2 adsorption solids.

1. Introduction

With the widespread use of the combustion of fossil fuels, exceeding 13 gigatonnes carbon dioxide (CO_2) annually has released into Earth's atmosphere (Banerjee et al., 2008). Those has caused a large number of environmental issues, such as a rising global average temperature and sea level (McDonald et al., 2015). It has recently been reported that the accumulation of CO_2 in atmosphere has reached the highest level in 400 000 years (Yang et al., 2013), from a concentration of 270 ppm in 1850 (Haszeldine, 2009) to more than 410 ppm in April 2018. Therefore, carbon capture and storage (CCS) technology has attracted significant attention to reduce and store excessive CO_2 emissions generated by burning fossil fuels (Broda & Müller, 2012; Rochelle, 2009). In recent decades, amine-scrubbing process is mainly used industrially for CCS technology of CO_2 adsorption by using aqueous amine-polymer (Choi et al., 2016; Figueroa, Fout, Plasynski, McIlvried, & Srivastava, 2008). However, there are several drawbacks with the uses of amine-scrubbing technique, such as large energy consumption, high cost and toxic (Jeon, Jung, Kim, & Lee, 2018). To overcome these limitations, there has been attracting attentions to novel solid adsorbents with higher stability and lower energy consumption (Gromov et al., 2018; Zhang, Zhu, Lin, Qi, & Chen, 2011).

The various solid sorbent materials with high specific surface area, such as zeolites (Bacsik, Cheung, Vasiliev, & Hedin, 2016), metal-organic frameworks (MOFs) (Darunte, Oetomo, Walton, Sholl, & Jones, 2016), aerogel (Han et al., 2017), porous polymer networks (Chen, Wang, Li, Fang, & Li, 2017), silica (Hahn et al., 2016) and porous carbons (Estevez et al., 2018), have been investigated extensively as adequate physical affinity for CO_2 even at low concentration of CO_2 condition. In order to improve the capacity of CO_2 adsorption further, the chemical grafting and the physical impregnation are two main methods to load the amine-polymer in the solid porous materials (Pang, Lee, Sakwa-Novak, Lively, & Jones, 2017). As for physical impregnation methods, the adsorption sorbents were prepared by impregnated aqueous amine-polymer into porous solids to chemisorb CO_2 with high CO_2 adsorption capacity and low energy consumption. Kishor and Ghoshal (2016) reported a novel PEI-impregnated into three dimensional mesoporous silica showing a high CO_2 adsorption capacity. However, the specific surface area of this silica drastically decreased by 93.3%, from 857 m^2/g to 57 m^2/g after loading PEI in silica. Guo, Ding, Kanamori, Nakanishi, and Yang (2017) had recently reported that a novel CO_2 sorbent was prepared by impregnation of PEI on silica monoliths. Similarly, the specific surface area of monoliths decreased by 99.9% (from 499 m^2/g to 0.5 m^2/g) when the concentration of PEI was 60 wt %. The large amount of PEI fills in the pore channels of porous sorbents reducing the accessibility of the interior of PEI molecules to CO_2 molecules, limiting CO_2 adsorption performance.

Compared with the physical impregnation, the chemical grafting based on covalent bond between amine species and porous materials can provide highly CO_2 adsorption sites and show good cycling stability

* Corresponding author.
E-mail address: Okubay@kit.ac.jp (S. Okubayashi).

https://doi.org/10.1016/j.carbpol.2019.115248
Received 19 July 2019; Received in revised form 23 August 2019; Accepted 23 August 2019
Available online 26 August 2019

(Chai, Liu, Huang, Tan, & Dai, 2016). Zhang, Guan, Wang, Yu, and Ding (2017) reported that the CO_2 adsorption capacity of PEI-grafted PAN membranes (1.5 mmol/g) was much higher than the PEI impregnated membranes (0.37 mmol/g) when both of the PEI content were 20 wt%. The specific surface area of PEI-grafted membranes (Zhang et al., 2017) decreased from 50.53 m^2/g to 16.79 m^2/g by 67% which was lower than that of PEI impregnated membranes decreased from 50.53 m^2/g to 7.22 m^2/g by 86%. The chemical grafting is more suitable method than the impregnation method to decrease the reduction range of specific surface area.

Among the various solid sorbent materials, cellulose aerogels have already attracted many attentions due to its outstanding properties, such as low-density, large specific surface area, renewable and biodegradable properties (Fu, Ansari, Zhou, & Berglund, 2018). Compared with the porous silica aerogel (Guo et al., 2017), a larger number of the hydroxyl group on the surface of the cellulose can form the hydrogen bond with the primary amine group of PEI (Chen et al., 2018), resulting in a higher amount of PEI loading. Moreover, the hydroxyl group of the cellulose could graft with PEI by adding crosslink agents to decrease the reduction range of specific surface area, increasing the CO_2 adsorption capacity. Therefore, cellulose aerogels may represent a promising matrix for combustion CO_2 capture.

In this study, we demonstrate a novel PEI-crosslinked cellulose (PCC) aerogel sorbent for combustion CO_2 capture by adding the glutaraldehyde (GA) as the crosslink agent. The obtained cellulose aerogels crosslinked by PEI showed 3D porous structure, large specific surface area and high CO_2 adsorption capacity as an excellent CO_2 adsorbent. This study aimed to compare the morphologies, specific surface area, and CO_2 capture performance of PCC aerogels with those of PEI-impregnated cellulose (PIC) aerogels. Besides, the influence of temperature on CO_2 adsorption, CO_2 adsorption kinetic and the CO_2 cycle adsorption characteristics of as-prepared materials were studied. This work is the first time to reveal that the PEI-crosslinked cellulose aerogel can be a potentially sorbent for combustion CO_2 capture.

2. Experimental section

2.1. Materials

Cellulose triacetate (CTA, DP = 300; DS = 2.85) was supplied by Daicel Corporation Co., Ltd, Japan. Polyethyleneimine (PEI, M_w = 600, 99%) with an average molecular mass of 600 was bought from Junsei Chemical Co., Ltd, Japan. Ethanol (99.5%), 1, 4-dioxane (≥99.5%), glutaraldehyde (GA, 25% in water) and sodium hydroxide (NaOH), were all purchased from Nacalai Tesque Co., Ltd, Japan and used without further purification. CO_2 used for supercritical drying and N_2 used for thermogravimetric analysis (TGA) were purchased from Kaindo Gas Co., Ltd., Japan. In this work, all water mentioned is distilled water produced by a water purification system (SA-2100E, Eyela, Japan).

2.2. Preparation of cellulose gels

Cellulose gels were prepared by hydrolyzing the cellulose triacetate (CTA) gels as showed in Fig. 1. Cellulose triacetate gels were prepared according to a method reported in the previous study (Cheng & Okubayashi, 2019): briefly, the CTA powder was placed in the oven for 2 h to remove moisture at 60 ℃. Afterward, 1 g of CTA was dissolved in 50 ml of 1, 4-dioxane solution under stirring for 3 h to get a homogeneous solution at 70 ℃. Then the ethanol of the same volume as 1, 4-dioxane was poured into the mixed homogeneous solution for another 5 h at 70 ℃. The designed concentration of CTA was 10 mg/cm^3. The hot mixed solution was poured into cylindrical molds with a diameter of 25 mm and cooled down to 20 ℃ to form CTA gels due to non-solvent and thermal induced phase separation. CTA gels were carefully removed from the molds and cut into cylinders with a thickness of 5 mm. The 1, 4-dioxane in the cylindrical CTA gel was removed and exchanged with ethanol by soaking into ethanol for 24 h at room temperature. Then the CTA ethanol-gel was hydrolyzed in a 0.05 M of sodium hydroxide (Ding et al., 2018) in a mixture of ethanol and water (3:1, V/V) for 3 h at room temperature and the solvent in the gel exchanged again with ethanol to remove water and to get the cellulose ethanl-gel.

2.3. Preparation of PIC and PCC aerogels

PEI-impregnated cellulose (PIC) gels were prepared by using wet impregnation methods (Guo et al., 2017). First, 1 g of PEI was dissolved in 10 ml of ethanol on a magnetic stirrer for 30 min. After that, a cylindrical cellulose ethanol-gel (diameter = 25 mm, thickness = 5 mm) was immersed into the PEI solution for 24 h to form PIC gels at room temperature. The preparation procedure of PEI-crosslinked cellulose (PCC) gels were schematically shown in Fig. 1. First, the obtained PIC gel was immersed into a mixture of ethanol and water (3/1, V/V) containing different amount of glutaraldehyde (GA, 0.1 wt%, 0.5 wt%, 1 wt%) at room temperature for 24 h. The brown PCC aerogels prepared from various the content of GA were denoted in Table 1 as PCC-0.1, PCC-0.5, PCC-1, respectively. Then, the cylindrical PCC gel was treated with ethanol to remove the water for four times to get PCC ethanol-gels.

In order to maintain the complete structure of aerogels, the cellulose, PIC and PCC ethanol-gels were dried using supercritical CO_2 which an equipment was showed in Fig. S1. The procedure was described briefly as follows: The high pressure vessel was heated at 40 ℃ in which the ethanol-gel was placed. Then the liquid CO_2 was filled in the high pressure vessel until the pressure reached at 15 MPa. The sample was dried for 150 min with a flow rate of 4 ml/min. Finally, the pressure in the vessel was released at two stage: to 10 MPa at rate of 1 MPa/min and to atmospheric pressure at rate of 0.2 MPa/min.

The thickness and the diameter of cylindrical aerogels were measured by using a millimeter to calculate the volume of aerogels. The volume shrinkage (S) of all aerogels was obtained according to the Eq. (1):

$$S(\%) = \frac{V_0 - V}{V_0} \times 100\% \quad (1)$$

where V_0 is the volume of ethanol-gels before drying, V is the volume of aerogel.

2.4. Characterization

The C, H, and N composition of the aerogel were determined through a Microcorder JM10 elemental analyzer (J. Science laboratory Co., Ltd., Japan). The morphology structure of all samples were studied by a scanning electron microscope in a JSM-6700F microscope (JEOL Ltd., Japan). The fourier-transform infrared spectroscopy (FTIR) spectra of all aerogels were obtained in the range 4000–600 cm^{-1} by using an attenuated total reflection accessory equipped in Spectrum One spectrometer (PerkinElmer Co., Ltd., Japan).

Before N_2 adsorption-desorption measurement, the samples were dried by using a pretreatment instruments (BELPREP-vac II, Microtrac BEL Co. ltd., Japan) at 100 ℃ for 3 h in a vacuum environment less than 1 Pa. N_2 adsorption-desorption isotherms were evaluated at −196 ℃ by using the BELSORP-mini II analyzer (Microtrac BEL Co. Ltd., Japan) and the specific surface area (S_{BET}) of aerogels were calculated at relative pressure between 0.05 and 0.3 based on Brunauer-Emmett-Teller (BET) model. It should be noted that the specific volume and the size distribution of pores in the bio-aerogels was measured using N_2 adsorption-desorption method based on BJH approach. The specific pore volume measured with BJH method does not take into account 90% of the pore volume as BJH approach only considers pores sizes below 200 nm (Rudaz et al., 2014). The average pore size (D_p) within cylindrical pores was calculated by the classical formula, $D_p = 4V_{pBJH}/$

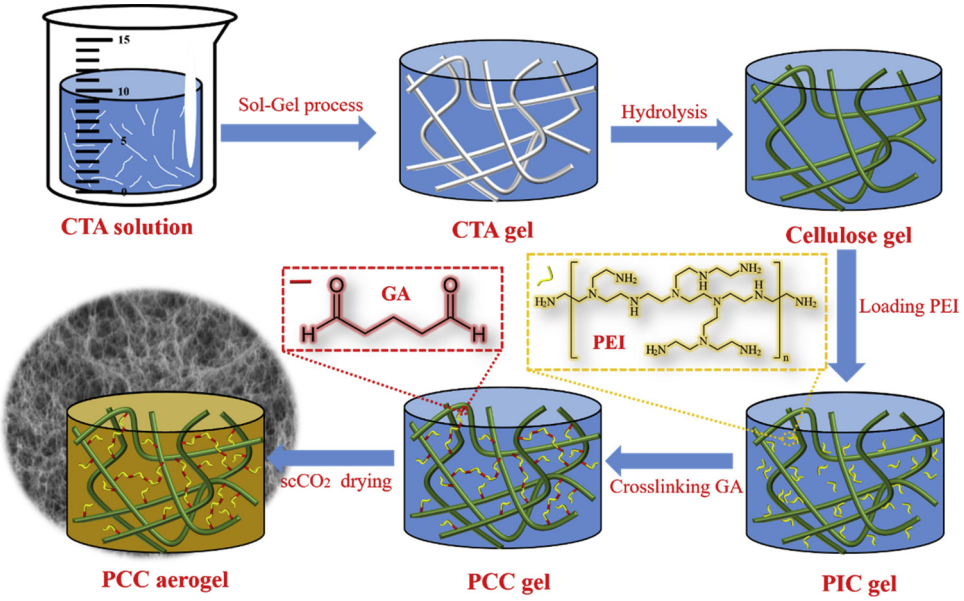

Fig. 1. A schematic illustration of the synthesis of porous PCC aerogels.

Table 1
Elemental components and physical properties of aerogels.

Sample	Elemental analysis			S[a] (%)	Density (mg/cm^3)	S_{BET}[b] (m^2/g)
	C (%)	H (%)	N (%)			
CTA	–	–	–	5.3	10.6	447.8
Cellulose	–	–	–	20.9	14.1	394.2
PIC	44.6	8.4	18.4	875.1	958.2	0.4
PCC-0.1	54.9	8.1	9.7	10.2	23.8	285.5
PCC-0.5	41.0	8.7	15.8	12.8	51.6	260.7
PCC-1	40.6	9.8	17.4	8.4	97.2	234.2

[a] Shrinkage calculated from Eq. (1).
[b] Specific surface area.

S_{BET}, where V_{pBJH} is the specific pore volume measured by N_2 adsorption-desorption method based on BJH method and S_{BET} is the specific surface area, which will strongly underestimate the values of D_p (Groult & Budtova, 2018). Thus, only the specific surface area of all aerogels are analyzed by N_2 adsorption-desorption method without calculated the specific pore volume and the average pore sizes.

2.5. Measurements of CO_2 adsorption

The CO_2 adsorption performance and cyclic performance of the PIC and PCC aerogels were studied by using the setup of thermogravimetric analyzer (Discovery TGA, TA instruments Co. Ltd., America) as shown in Fig. S2. In this test, approximately 10 mg of dried aerogels was loaded into a microbalance alumina sample pan. Before adsorption measurement, the sample was heated from room temperature to 100 °C in pure N_2 to remove the water and impurities adsorbed for 60 min. Then the CO_2 adsorption capacity of samples was measured by switching pure dry CO_2 (200 ml/min) for 70 min. The measurement of CO_2 adsorption was carried out at different temperatures at 25, 40, 60 and 75 °C to study the impact of temperature on the adsorption kinetic. For desorption process, the temperature was increased to 105°C with introducing pure N_2 and lasted for 40 min. For evaluation of the CO_2 adsorption regeneration properties of the aerogel, the sample was continued to measure for 10 cycles. This recycle evaluation was performed with adsorption at 40 °C under CO_2 atmosphere for 70 min and desorption at 105 °C under N_2 atmosphere for 40 min. The adsorption capacity (mmol/g) was calculated by the weight variation of samples during the measurement of CO_2 adsorption.

3. Results and discussion

Fig. 1 depicts the fabrication process of the PEI-crosslinked cellulose (PCC) aerogel with three dimensional and nanoporous structure based on two crucial processes. The first process was preparation of cellulose gels with hydrolyzing the cellulose triacetate (CTA) gel obtained by sol-gel process. The formation of CTA gels was due to the phase separation which is based on the existence of non-solvent and decreasing temperature as we had reported (Cheng & Okubayashi, 2019). In this method, the shape of samples was controlled by using the different molds as shown in Fig. S3, which is significant for practical application. The second procedure was crosslinking the polyethyleneimine (PEI) with cellulose gels by using the different content of glutaraldehyde (GA). If PEI impregnated into the cellulose gel without the crosslinking, the PEI-impregnated cellulose (PIC) aerogel was not stable in the air. Even though the PIC aerogel retained the monolith shape and morphology after drying by supercritical carbon dioxide, it showed large shrinkage under atmosphere condition after 24 h and the color of sample changed from white to yellow as indicated in Fig. S4. After adding the crosslinking agent GA, the PCC aerogel became stable also as shown in Fig. S4.

3.1. FTIR measurement

Fig. 2a represents the expecting chemical structure of the PCC aerogel and its reaction scheme for chemisorb CO_2. The conversion of characteristic groups in this process was identified by FT-IR analysis as shown in Fig. 2b. The strong characteristic peak near 1737 cm^{-1} and 1214 cm^{-1}, which assigned to C = O and C–O–C stretching vibration of the acetyl group, disappeared in the spectrum of cellulose. Additionally, the FT-IR spectrum of cellulose aerogel displayed the presence of the broad absorbance peak around 3200-3680 cm^{-1}. These peaks belonged to the stretching vibration of O–H which appeared after the hydrolysis, indicating the acetyl group of CTA was hydrolyzed with alkali treatment (Han, Lu et al., 2019). After PEI loading in the cellulose gel to form PIC aerogel, some new peaks evolved at 1300–1700 cm^{-1} which confirms the presence of PEI in the aerogel. The absorbance peaks near 1560 cm^{-1} and 1469 cm^{-1} are also contribution of N–H stretching vibration of primary amines in PEI (Wang et al., 2009). After crosslinking

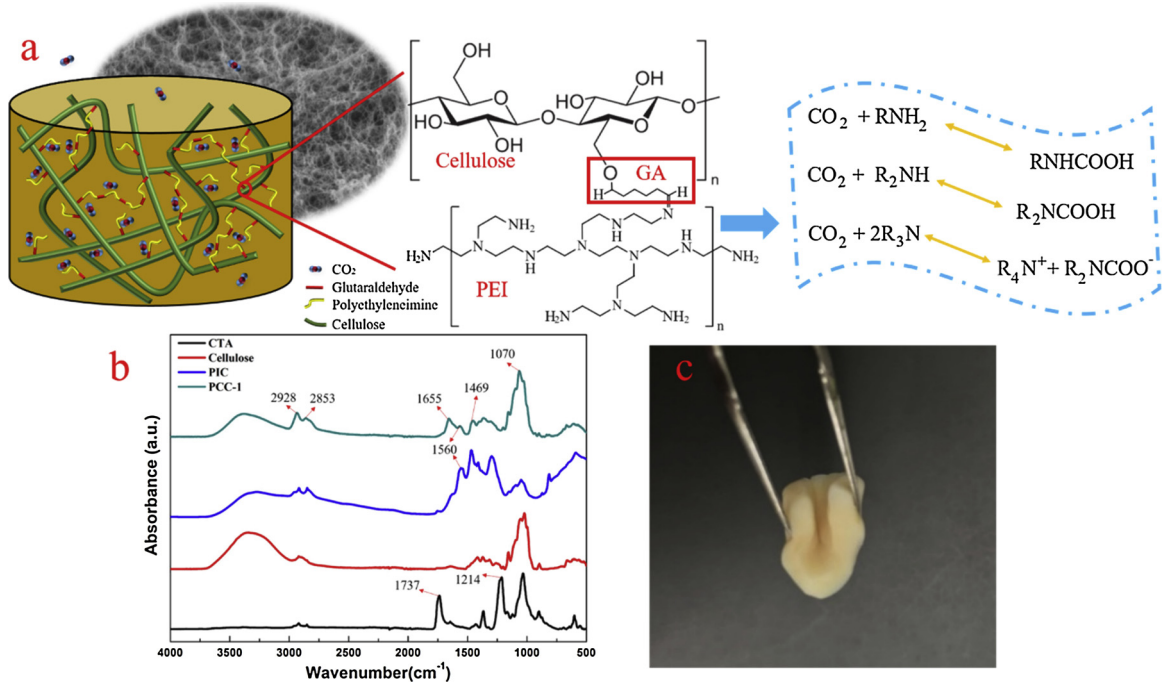

Fig. 2. (a) A schematic depiction of the chemical structure of PCC aerogel for CO_2 chemisorption; (b) FT-IR spectra of CTA, Cellulose, PIC and PCC-1 aerogels; (c) Photo image of flexible PCC-0.1.

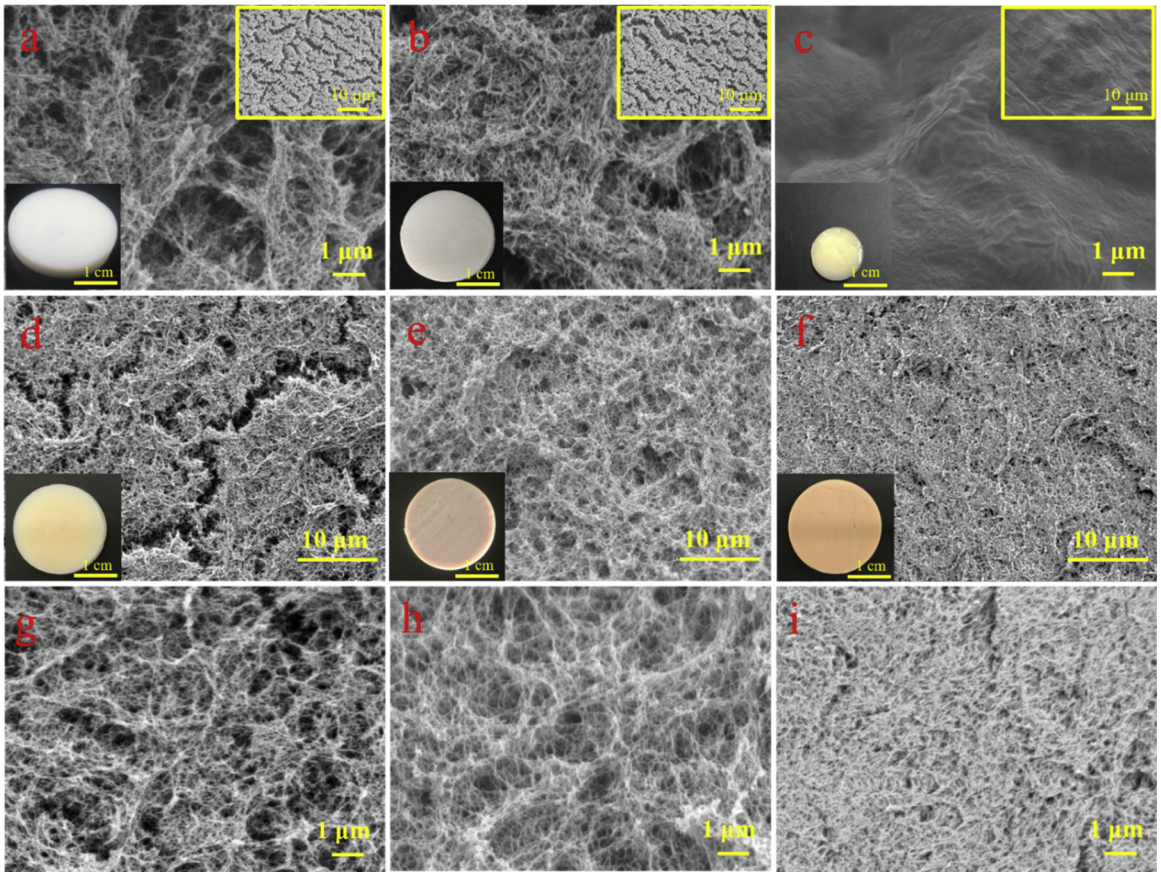

Fig. 3. The FE-SEM image of (a) CTA aerogel; (b) cellulose aerogel; (c) PIC aerogel; (d), (g) PCC-0.1 aerogel; (e), (h) PCC-0.5 aerogel; (f), (i) PCC-1 aerogel.

of PIC with GA i.e. PCC-1 has new peaks near 1655 cm^{-1}. These peaks are assigned to the stretching of C=N group produced in the glutaraldehyde crosslinking process as reported (Zhang, Zang, Shi, Yu, & Sheng, 2016). Compared with the spectra of PIC aerogel, PCC aerogel had a great enhancement in absorbance of C–O skeleton vibration at 1070 cm^{-1} and the bending vibration of $–CH_2$ around 2853 cm^{-1} and 2928 cm^{-1}, indicating the PEI was successfully introduced to the cellulose aerogel. Notably, PCC aerogel obtained by crosslinking reaction

showed a certain degree of flexibility as demonstrate in Fig. 2c, unlike the brittle CTA or cellulose aerogel, which is very important in application.

3.2. Characteristic of aerogels

The element contents of C, H and N in PIC and PCC aerogels are listed in Table 1. The PIC and PCC aerogels showed high N content in the range of 9.7–18.4 %, due to the high N content of PEI impregnated in the aerogel. The N content of PCC increased significantly from 9.7% to 17.4% as the GA concentration increased because the higher GA content promoted crosslinking of PEI and cellulose. However, the mixture solution of PEI and GA formed a new gel to prevent PEI from entering PIC gel when the GA concentration was more than 1 wt% as exhibited in Fig. S5. In this process, successful crosslinking of PEI with cellulose aerogel was confirmed by both results of the elemental analysis and FTIR. The higher nitrogen content would be beneficial for chemisorb CO_2 (Didas, Choi, Chaikittisilp, & Jones, 2015).

After supercritical CO_2 drying, CTA aerogel showed the lowest density as given in Table 1, indicating the lowest shrinkage, that is less than 6%, maybe due to its hydrophobic property. After alkaline hydrolysis process, the shrinkage of cellulose aerogel increased to 21% due to hydroxyl groups on the cellulose surface as detected by FTIR analysis as given in Fig. 2b. PIC aerogel showed drastically larger shrinkage over 800% as seen in Fig. S4 when a larger amount of PEI impregnated into the cellulose due to the capillary force as the PEI and absorption water were liquid (Cheng et al., 2017). This larger shrinkage resulted in drastically higher density of PIC. On the other hands, PCC aerogel showed smaller shrinkage in the range of 8.4–12.8 % than cellulose aerogel as the hydroxyl group of cellulose participated in the crosslinking reaction, resulting in reduction of shrinkage.

3.3. Morphology characterization

The morphology of aerogels was observed by FE-SEM as shown in Fig. 3. Both CTA (Fig. 3a) and cellulose aerogels (Fig. 3b) have three-dimensional (3D) and randomly oriented structure with irregularly shaped microscale and nanoscale pores, which was quite similar structure to regenerated polymer aerogels (Ulker & Erkey, 2014; Yue, Zhang, Yang, Qiu, & Li, 2018). The aerogel prepared from the mixture of cellulose and PEI, PIC exhibited a composite structure without any pores due to the severe contraction caused by capillary force; simultaneously, the color of the aerogel changed from white to light yellow (inset of Fig. 3c) as the color of PEI was yellow. As displayed in Fig. 3d–f, PCC aerogels still retained three-dimensional structure with irregularly shaped microscale and nanoscale pores, showing that the morphology of cellulose aerogel did not damage during the crosslinking process. FE-SEM images with high-magnification (Fig. 2g–i) clearly showed that the amount of microscale pores in PCC aerogels were less than CTA and cellulose aerogel. Those results could be speculated that the PEI (yellow line in Fig. 2a) crosslinked in the pore of cellulose by GA (red line in Fig. 2a) in the microscale pore of cellulose aerogel (green line in Fig. 2a) to convert the microscale pores to nanoscale pores as shown in Fig. 2a. As the content of GA increased from 0.1% to 1%, the color of PCC aerogel showed the deeper yellow (the inset of Fig. 3d–f). And the pore size in PCC aerogel was more uniform when the concentration of GA increased (Fig. 3d–f).

3.4. BET measurement

For further evaluation of pore structure of the aerogel, N_2 adsorption-desorption isotherms were obtained for the aerogels at 77 K. The results were shown in Fig. 4. The curves of CTA and cellulose aerogel showed type-IV adsorption-desorption isotherm with an obvious H3 hysteresis loop as same as the typical regenerated cellulose aerogel (Gao et al., 2018), suggesting the open and continuous pores in the aerogel. In comparison of specific surface area as given in Table 1, CTA (447.8 m^2/g) was a little larger than the cellulose (394.2 m^2/g) due to the smaller shrinkage. The curves of PIC aerogel in the Fig. 4a presented that the N_2 adsorption capacity significantly decreased after PEI loading in cellulose; simultaneously, the specific surface area of PIC aerogel (0.4 m^2/g) had a sharp decline due to the large shrinkage. The decline phenomenon also had report in the hierarchically porous silica monoliths (Guo et al., 2017) and MOF-derived carbon monolith (Gadipelli, Patel, & Guo, 2015) due to the penetration of PEI in the pore of porous materials, limiting CO_2 adsorption performance. Fig. 4b represents the N_2 adsorption-desorption isotherms of PCC aerogels, showing type IV with characteristics hysteresis loop. This mesopores adsorption characteristic in PCC aerogel, such as monolayer adsorption, multilayer adsorption, and capillary condensation phenomenon, were observed to be helpful for CO_2 adsorption (Si, Ren, Li, Ding, & Yu, 2012). Typically, the amount of N_2 adsorption showed an abrupt rise when p/p_0 is larger than 0.8 as the gas deposits in the nanoscale pore of PCC aerogel. Moreover, the specific surface area of PCC aerogel in the range of 234.2-285.5 m^2/g as given in Table 1, retained more than 60% of cellulose aerogel, far larger than 33% of PEI-grafted electrospinning PVN membranes (Zhang et al., 2017) and 1% of PEI-impregnated porous silica (Guo et al., 2017). Additionally, the hysteresis loop of PCC aerogel was changed to type H4 compared with CTA and cellulose aerogels showing type H3, suggesting the continuous open pores and the uniform pore size (Sing & Williams, 2004) that was observed by SEM in Fig. 3. Such PCC aerogel with 3D porous structure and large specific surface area would be conducive to physical adsorption of CO_2 (Han, Wang et al., 2019).

3.5. CO_2 adsorption performance and kinetic analysis

CO_2 adsorption-desorption performance of PCC aerogels were investigated through TGA method with using pure dry CO_2 at different adsorption temperatures. Fig. 5(a) represents CO_2 adsorption-desorption capacity of PCC-0.1, PCC-0.5 and PCC-1 aerogels reached at 0.9, 1.5 and 2.1 mmol/g at 40℃ respectively, potentially reducing the cost of CO_2 sequestration (Yang, Li, Chen, Zhao, & Li, 2010). PCC-1 aerogel showed the larger CO_2 adsorption capture than PCC-0.1 and PCC-0.5 aerogels as it had the larger N content shown in the Table 1. More N content can form more covalent bond with CO_2 to show larger CO_2 adsorption. However, the CO_2 adsorption capacity of PIC aerogel only reached at 0.4 mmol/g at 40 ℃ as demonstrated in Fig. S6 because the large shrinkage of PIC aerogel destroyed the porous structure and blocked the channel of CO_2 adsorption. Additionally, it was obviously found that the adsorption curves of all PIC and PCC aerogels obviously showed two stage adsorption, including a fast adsorption and a slow adsorption, which usually occurred in amine-functionalized porous materials (Li & Tezel, 2007).

The adsorption temperature usually has a significant effect on the adsorption capacity due to chemical adsorption and physical adsorption (Zhang et al., 2017). Fig. 5b shows the CO_2 adsorption capacities of PCC-1 aerogels from 25 ℃ to 75 ℃. It could be seen that the amount of the CO_2 adsorption decreased when the temperature increased as the covalent bond between CO_2 and amine groups was weakened at high temperature. In addition, the monolayer adsorption, multilayer adsorption, condensation capacity of CO_2 also decreased at high temperature according to the principle of thermodynamics. The adsorption kinetic parameters of PCC aerogels were evaluated by using the pseudo-first kinetic order and pseudo-second kinetic order as shown in the Table 2.

The pseudo-first order model has been widely used to predict adsorption kinetic (Serna-Guerrero & Sayari, 2010) which is expressed as:

$$q_t = q_e(1 - e^{-k_f t}) \quad (2)$$

where q_t (mmol/g) is the adsorption capacities at a given time, q_e

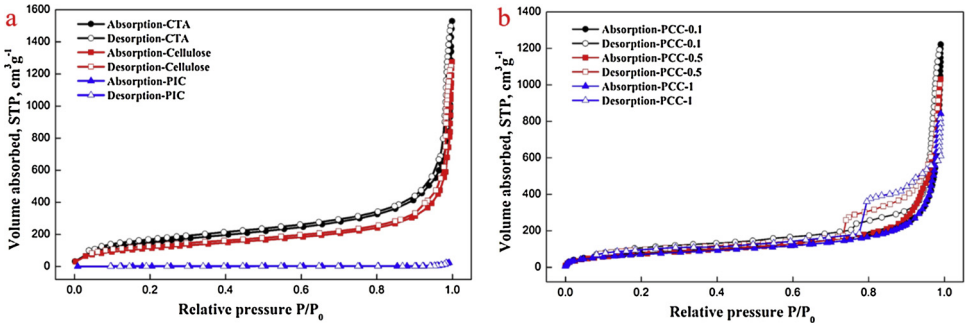

Fig. 4. N_2 adsorption-desorption isotherm of CTA, Cellulose and PIC aerogels (a) and PCC aerogels (b).

(mmol/g) is the adsorption capacities at equilibrium, k_f (min^{-1}) is the first order kinetic constant and t is the time. Pseudo-first order model is suitable to predict the adsorption behavior between sorbent and gas based on physical adsorbents. The values of k_f, q_e and correlation coefficient R^2 obtained are presented in Table 2. The R^2 value at different temperatures were found to be relatively small, in the range of 0.85 to 0.90. Besides, it was also observed that the estimated q_e values is lower than that of the experimental (q_{ee}) values. Those showed that the adsorption of PCC aerogels was bad fitted to pseudo-first order model.

The pseudo-second order model (Ho & McKay, 1999) was also applied to predict adsorption kinetic which is expressed as:

$$\frac{t}{q_t} = \frac{1}{k_s q_e^2} + \frac{t}{q_e} \tag{3}$$

where q_t (mmol/g) is the adsorption capacities at a given time, q_e (mmol/g) is the adsorption capacities at equilibrium, k_s (min^{-1}) is the second order kinetic constant and t is the time. Pseudo-second order model was suited to describe the adsorption behavior involved chemical interactions by the strong binding between CO_2 and the adsorbent (Hameed, Tan, & Ahmad, 2008). The correlation coefficient R^2 of all samples were almost close to 1 at different temperatures, showing that the pseudo-second order kinetic model is suitable to describe the adsorption process of PCC aerogels involving chemical adsorption. It was also observed that the second order rate constant (k_s) increased when adsorption temperature increased, indicating the enhanced of CO_2 molecular mobility. The CO_2 molecular was more active and harder to be adsorbed into the aerogel at high adsorption temperature, resulting in the decline of CO_2 adsorption capacity. To verify that CO_2 was successfully adsorbed into the PCC aerogel, the FT-IR spectra of PCC-0.1 aerogel with largest specific surface area was also conducted to be compared after CO_2 adsorption (Fig. 5c). The absorption peak at 1324–1388 cm^{-1} and 1423–1476 cm^{-1}, which could be belonged to bicarbonate and monodentate carbonate respectively (Song et al., 2016). Additionally, a small peak at 2303 cm^{-1} could be found after adsorption, which was assigned to the stretching vibration of CO_2, indicating the existence of physical adsorption (Zhang et al., 2017). As a

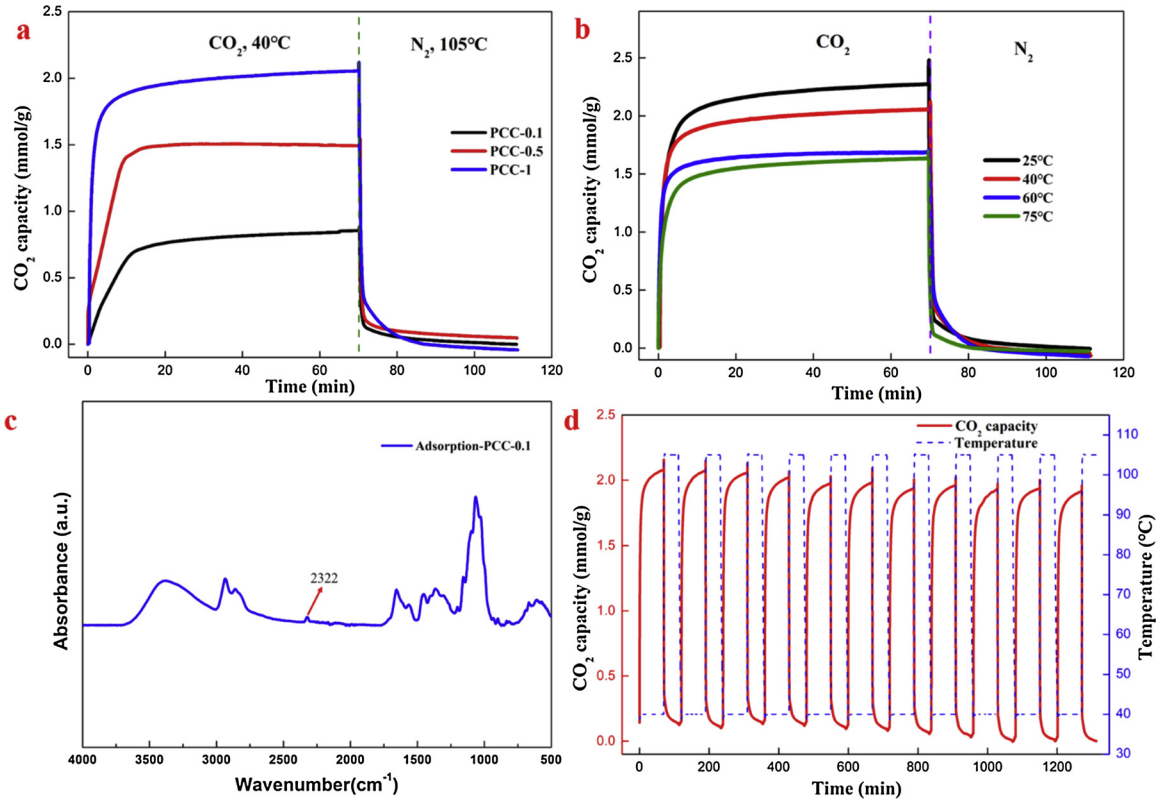

Fig. 5. CO_2 adsorption-desorption isotherm of PCC-0.1, PCC-0.5 and PCC-1 aerogels performed at 40°C for adsorption and 105°C for desorption (a), and PCC-1 aerogel at different adsorption temperatures (b); (c) FT-IR spectra of PCC-0.1 aerogel after CO_2 adsorption; (d) CO_2 adsorption-desorption cyclic isotherm of PCC-1 performed at 40°C for adsorption and 105°C for desorption.

Table 2
Parameters of pseudo-first order, pseudo-second order models and intra-particle diffusion model of PCC-1 aerogel under different adsorption temperatures.

Temperature (°C)	q_{ee} (mmol/g)	Pseudo-first order model			Pseudo-second order model			Intra-particle diffusion model		
		k_f (min^{-1})	q_e (mmol/g)	R^2	k_s (min^{-1})	q_e (mmol/g)	R^2	k_i (mmol/g·$min^{0.5}$)	C(mmol/g)	R^2
25	2.37	0.53	2.19	0.90	0.32	2.31	0.98	0.39	2.01	0.97
40	2.10	0.67	1.89	0.89	0.43	2.08	0.99	0.33	1.73	0.98
60	1.73	1.25	1.45	0.86	0.95	1.70	0.99	0.17	1.59	0.95
75	1.69	1.39	1.37	0.85	0.99	1.66	0.99	0.22	1.45	0.97

Table 3
Comparison of structure parameters and adsorption capacity between the PCC aerogel and the previous reports.

Sample	S_{BET} (m^2/g)	Adsorption temperature (°C)	CO_2 adsorption amount (mmol/g)	Ref.
Hierarchically silica monolith	0.5	25	1.01	Guo et al. (2017)
Hydrolyzed PAN membranes-PEI	16.8	25	1.50	Zhang et al. (2017)
supramolecular organic framework	21	25	1.49	Hwang, Park, Kim, and Lee (2018)
NH_2-MCM-36	145	25	1.2	Yang et al. (2012)
Pore-expanded MCM-41 silica-PEI	16.7	25	1.7	Heydari-Gorji, Belmabkhout, and Sayari (2011)
TEMPO-cellulose-PEI foaming	8.3	75	2.22	Sehaqui et al. (2015)
PCC-1	234.2	25	2.31	This work

result, it could be found that the CO_2 adsorption mechanism on PCC aerogels was the combination of chemical and physical adsorption.

As pseudo-first order and pseudo-second order were not able to investigate the diffusion mechanism, Weber and Morris (1962) proposed a simplest approximation of the pore diffusion kinetics, intra-particle diffusion model, to study the adsorption mechanism. It is expressed as:

$$q_t = k_i t^{\frac{1}{2}} + C \quad (4)$$

where C is the intercept and Ki (mmol/g $min^{1/2}$) is the intra-particle diffusion rate constant. If the curve of q_t and t shows linear relationship, the adsorption process involves in the intra-particle diffusion; if the curve passes through the origin, the intra-particle diffusion is the only rate-limiting step. Otherwise, some other mechanism with intra-particle diffusion may be operating simultaneously. It could be observed that all the curves of PCC-1 aerogel exhibited twin-linearity at different adsorption temperatures (Fig. S7). The same phenomenon could be also found in the porous MgO for CO_2 adsorption, suggesting that two rate-limiting steps occurred in the adsorption process (Hameed et al., 2008). The initial stage of curve represents surface diffusion from gas phase to the exterior of PCC aerogels; the second linear section represents the sluggish diffusion in pore structure of PCC aerogels where intra-particle diffusion is rate-limiting. It is also found that the intercept C (Table 2) decreased with increasing adsorption temperature, suggesting the thickness of boundary layer decreased as the molecular motion increase at high temperature.

The cyclic performance of CO_2 adsorption materials is also important for practical application as it directly reduced the cost of CO_2 adsorption. The CO_2 cyclic isotherm of PCC-1 aerogel at 40 °C adsorption with 105 °C desorption are presented in Fig. 5d. After 10 cyclic experiments, the CO_2 capacity do not significantly reduce at a desorption temperature of 105 °C, still retaining 93% of the initial value as shown in Fig. S8. The PCC aerogel showed excellent cyclic performance because of the crosslinking reaction which the amine groups of PEI was fixed to the network of cellulose by GA as shown in Fig. 2a. Table 3 showed the comparison of structure parameters and adsorption capacity between the PCC aerogel and the previous reports. It could be concluded that the PCC aerogel showed high CO_2 adsorption capacity, fast adsorption kinetics and excellent recyclability with the chemical and physical adsorption. Additionally, the controllable shape, high N content, porous structure and high specific surface area showed that the PCC aerogel played an important role in combustion CO_2 capture.

4. Conclusions

The flexible and porous PCC aerogel was synthesized by a novel strategy with the sol-gel process, the hydrolysis reaction and the crosslinking reaction. All PCC aerogels showed the three-dimensional (3D) irregularly shaped microscale and nanoscale pores with high specific surface area. The PCC-1 aerogel had the maximum adsorption capacity at 2.31 mmol/g at 25 °C under pure dry CO_2 based on the chemical and physical adsorption. When the adsorption temperature increased, CO_2 adsorption capacity of PCC aerogel decreased. The CO_2 adsorption-desorption curve showed two-stage adsorption with a fast initial step and a slow following step. Pseudo-second order model was suitable to describe the adsorption process of PCC aerogels and both of the surface diffusion and intra-particle diffusion were the rate-limiting. Additionally, the PCC-1 aerogel showed excellent CO2 adsorption-desorption recyclability after 10 adsorption-desorption cycle tests, indicating it is a potential solid adsorption materials in combustion CO_2 capture. This study will provide the way to understand the high CO_2 adsorption capture, excellent cycling stability and adsorption kinetics of the porous PCC aerogels as a potential CO_2 adsorption materials.

Acknowledgments

C.W. is gratefully acknowledged to the China Scholarship Council (CSC) for supporting his PhD research. The materials characterization, such as SEM, FTIR and BET measurement, are supported by Prof. Hiroyuki Yano, Kyoto University, which is gratefully acknowledged.

Appendix A. Supplementary data

Supplementary material related to this article can be found, in the online version, at doi:https://doi.org/10.1016/j.carbpol.2019.115248.

References

Banerjee, R., Phan, A., Wang, B., Knobler, C., Furukawa, H., O'Keeffe, M., et al. (2008). High-throughput synthesis of zeolitic imidazolate frameworks and application to CO_2 capture. *Science, 319*, 939–943.
Broda, M., & Müller, C. R. (2012). Synthesis of highly efficient, Ca-based, Al_2O_3-stabilized, carbon gel-templated CO_2 sorbents. *Advanced Materials, 24*, 3059–3064.
Bacsik, Z., Cheung, O., Vasiliev, P., & Hedin, N. (2016). Selective separation of CO_2 and CH_4 for biogas upgrading on zeolite NaKA and SAPO-56. *Applied Energy, 162*, 613–621.
Chai, S. H., Liu, Z. M., Huang, K., Tan, S., & Dai, S. (2016). Amine functionalization of microsized and nanosized mesoporous carbons for carbon dioxide capture. *Industrial*

& Engineering Chemistry Research, 55, 7355–7361.
Choi, W., Min, K., Kim, C., Ko, Y. S., Jeon, J. W., Seo, H., et al. (2016). Epoxide-functionalization of polyethyleneimine for synthesis of stable carbon dioxide adsorbent in temperature swing adsorption. *Nature Communications, 7*, 12640–12648.
Cheng, H., Gu, B., Pennefather, M. P., Nguyen, T. X., Phan-Thien, N., & Duong, H. M. (2017). Cotton aerogels and cotton-cellulose aerogels from environmental waste for oil spillage cleanup. *Materials & Design, 130*, 452–458.
Chen, C., Wang, H., Li, S., Fang, L., & Li, D. (2017). Reinforcement of cellulose nanofibers in polyacrylamide gels. *Cellulose, 24*, 5487–5493.
Chen, C., Mo, M., Chen, W., Pan, M., Xu, Z., Wang, H., et al. (2018). Highly conductive nanocomposites based on cellulose nanofiber networks via NaOH treatments. *Composites Science and Technology, 156*, 103–108.
Cheng, W., & Okubayashi, S. (2019). 3D aerogel of cellulose triacetate with supercritical antisolvent process for drug delivery. *The Journal of Supercritical Fluids, 148*, 33–41.
Didas, S. A., Choi, S., Chaikittisilp, W., & Jones, C. W. (2015). Amine–oxide hybrid materials for CO2 capture from ambient air. *Accounts of Chemical Research, 48*, 2680–2687.
Darunte, L. A., Oetomo, A. D., Walton, K. S., Sholl, D. S., & Jones, C. W. (2016). Direct air capture of CO2 using amine functionalized MIL-101 (Cr). *ACS Sustainable Chemistry & Engineering, 4*, 5761–5768.
Ding, Q., Xu, X., Yue, Y., Mei, C., Huang, C., Jiang, S., et al. (2018). Nanocellulose-mediated electroconductive self-healing hydrogels with high strength, plasticity, viscoelasticity, stretchability, and biocompatibility toward multifunctional applications. *ACS Applied Materials & Interfaces, 10*, 27987–28002.
Estevez, L., Barpaga, D., Zheng, J., Sabale, S., Patel, R. L., Zhang, J., et al. (2018). Hierarchically porous carbon materials for CO_2 capture: The role of pore structure. *Industrial & Engineering Chemistry Research, 57*, 1262–1268.
Figueroa, J. D., Fout, T., Plasynski, S., McIlvried, H., & Srivastava, R. D. (2008). Advances in CO_2 capture technology the US Department of Energy's Carbon Sequestration Program. *International Journal of Greenhouse Gas Control, 2*, 9–20.
Fu, Q., Ansari, F., Zhou, Q., & Berglund, L. A. (2018). Wood nanotechnology for strong, mesoporous, and hydrophobic biocomposites for selective separation of oil/water mixtures. *ACS Nano, 12*, 2222–2230.
Gadipelli, S., Patel, H. A., & Guo, Z. (2015). An ultrahigh pore volume drives up the amine stability and cyclic CO_2 capacity of a solid-amine @ carbon sorbent. *Advanced Materials, 27*, 4903–4909.
Guo, X., Ding, L., Kanamori, K., Nakanishi, K., & Yang, H. (2017). Functionalization of hierarchically porous silica monoliths with polyethyleneimine (PEI) for CO_2 adsorption. *Microporous and Mesoporous Materials, 245*, 51–57.
Groult, S., & Budtova, T. (2018). Thermal conductivity/structure correlations in thermal super-insulating pectin aerogels. *Carbohydrate Polymers, 196*, 73–81.
Gao, K., Guo, Y., Niu, Q., Fang, H., Zhang, L., Zhang, Y., et al. (2018). Effects of chitin nanofibers on the microstructure and properties of cellulose nanofibers/chitin nanofibers composite aerogels. *Cellulose, 25*, 4591–4602.
Gromov, A. V., Kulur, A., Gibson, J. A. A., Mangano, E., Brandani, S., & Campbell, E. E. B. (2018). Carbon nanotube/PVA aerogels impregnated with PEI: Solid adsorbents for CO_2 capture. *Sustain. Energy Fuels, 2*, 1630–1640.
Ho, Y. S., & McKay, G. (1999). Pseudo-second order model for sorption processes. *Process Biochemistry, 34*, 451–465.
Hameed, B. H., Tan, I. A. W., & Ahmad, A. L. (2008). Adsorption isotherm, kinetic modeling and mechanism of 2, 4, 6-trichlorophenol on coconut husk-based activated carbon. *Chemical Engineering Journal, 144*, 235–244.
Haszeldine, R. S. (2009). Carbon capture and storage: How green can black be? *Science, 325*, 1647–1652.
Heydari-Gorji, A., Belmabkhout, Y., & Sayari, A. (2011). Polyethylenimine-impregnated mesoporous silica: Effect of amine loading and surface alkyl chains on CO_2 adsorption. *Langmuir, 27*, 12411–12416.
Hahn, M. W., Jelic, J., Berger, E., Reuter, K., Jentys, A., & Lercher, J. A. (2016). Role of amine functionality for CO_2 chemisorption on silica. *The Journal of Physical Chemistry B, 120*, 1988–1995.
Han, J., Yue, Y., Wu, Q., Huang, C., Pan, H., Zhan, X., et al. (2017). Effects of nanocellulose on the structure and properties of poly (vinyl alcohol)-borax hybrid foams. *Cellulose, 24*, 4433–4448.
Hwang, K. S., Park, H. Y., Kim, J. H., & Lee, J. Y. (2018). Fully organic CO_2 absorbent obtained by a Schiff base reaction between branched poly(ethyleneimine) and glutaraldehyde. *The Korean Journal of Chemical Engineering, 35*, 798–804.
Han, J., Lu, K., Yue, Y., Mei, C., Huang, C., Wu, Q., et al. (2019). Nanocellulose-templated assembly of polyaniline in natural rubber-based hybrid elastomers toward flexible electronic conductors. *Industrial Crops and Products, 128*, 94–107.
Han, J., Wang, H., Yue, Y., Mei, C., Chen, J., Huang, C., et al. (2019). A self-healable and highly flexible supercapacitor integrated by dynamically cross-linked electro-conductive hydrogels based on nanocellulose-templated carbon nanotubes embedded in a viscoelastic polymer network. *Carbon, 149*, 1–18.
Jeon, S., Jung, H., Kim, S. H., & Lee, K. B. (2018). Double-layer structured CO_2 adsorbent functionalized with modified polyethyleneimine for high physical and chemical stability. *ACS Applied Materials & Interfaces, 10*, 21213–21223.
Kishor, R., & Ghoshal, A. K. (2016). High molecular weight polyethyleneimine functionalized three dimensional mesoporous silica for regenerable CO_2 separation. *Chemical Engineering Journal, 300*, 236–244.
Li, P., & Tezel, F. H. (2007). Equilibrium and kinetic analysis of CO_2-N_2 adsorption separation by concentration pulse chromatography. *Journal of Colloid and Interface Science, 313*, 12–17.
McDonald, T. M., Mason, J. A., Kong, X., Bloch, E. D., Gygi, D., Dani, A., et al. (2015). Cooperative insertion of CO_2 in diamine-appended metal-organic frameworks. *Nature, 519*, 303–308.
Pang, S. H., Lee, L. C., Sakwa-Novak, M. A., Lively, R. P., & Jones, C. W. (2017). Design of aminopolymer structure to enhance performance and stability of CO_2 sorbents: Poly (propylenimine) vs poly-(ethylenimine). *Journal of the American Chemical Society, 139*, 3627–3630.
Rochelle, G. T. (2009). Amine scrubbing for CO_2 capture. *Science, 325*, 1652–1654.
Rudaz, C., Courson, R., Bonnet, L., Calas-Etienne, S., Sallée, H., & Budtova, T. (2014). Aeropectin: Fully biomass-based mechanically strong and thermal superinsulating aerogel. *Biomacromolecules, 15*, 2188–2195.
Sing, K. S. W., & Williams, R. T. (2004). Physisorption hysteresis loops and the characterization of nanoporous materials. *Adsorption Science and Technology, 22*, 773–782.
Serna-Guerrero, R., & Sayari, A. (2010). Modeling adsorption of CO_2 on amine-functionalized mesoporous silica. 2: Kinetics and breakthrough curves. *Chemical Engineering Journal, 161*, 182–190.
Si, Y., Ren, T., Li, Y., Ding, B., & Yu, J. (2012). Fabrication of magnetic polybenzoxazine-based carbon nanofibers with Fe_3O_4 inclusions with a hierarchical porous structure for water treatment. *Carbon, 50*, 5176–5185.
Sehaqui, H., Gálvez, M. E., Becatinni, V., Cheng, Y., Steinfeld, A., Zimmermann, T., et al. (2015). Fast and reversible direct CO_2 capture from air onto all-polymer nanofibrillated cellulose polyethylenimine foams. *Environmental Science & Technology, 49*, 3167–3174.
Song, G., Zhu, X., Chen, R., Liao, Q., Ding, Y., & Chen, L. (2016). An investigation of CO_2 adsorption kinetics on porous magnesium oxide. *Chemical Engineering Journal, 283*, 175–183.
Ulker, Z., & Erkey, C. (2014). An emerging platform for drug delivery: Aerogel based systems. *Journal of Controlled Release, 177*, 51–63.
Weber, W., & Morris, J. (1962). Advances in Water pollution research: Removal of biologically resistant pollutants from waste waters by adsorption. *Proceedings of the International Conference on Water Pollution Symposium,* 231–266.
Wang, X., Schwartz, V., Clark, J. C., Ma, X., Overbury, S. H., Xu, X., et al. (2009). Infrared study of CO_2 sorption over "molecular basket" sorbent consisting of polyethylenimine-modified mesoporous molecular sieve. *The Journal of Physical Chemistry C, 113*, 7260–7268.
Yang, Y., Li, H., Chen, S., Zhao, Y., & Li, Q. (2010). Preparation and characterization of a solid amine adsorbent for capturing CO_2 by grafting allylamine onto PAN Fiber. *Langmuir, 26*, 13897.
Yang, S. T., Kim, J. Y., Kim, J., & Ahn, W. S. (2012). CO_2 capture over amine-functionalized MCM-22, MCM-36 and ITQ-2. *Fuel, 97*, 435–442.
Yang, S., Zhan, L., Xu, X., Wang, Y., Ling, L., & Feng, X. (2013). Graphene-based porous silica sheets impregnated with polyethyleneimine for superior CO_2 capture. *Advanced Materials, 25*, 2130–2134.
Yue, X., Zhang, T., Yang, D., Qiu, F., & Li, Z. (2018). Hybrid aerogels derived from banana peel and waste paper for efficient oil absorption and emulsion separation. *Journal of Cleaner Production, 199*, 411–419.
Zhang, J. P., Zhu, A. X., Lin, R. B., Qi, X. L., & Chen, X. M. (2011). Pore surface tailored SOD-Type metal-organic zeolites. *Advanced Materials, 23*, 1268–1271.
Zhang, N., Zang, G. L., Shi, C., Yu, H., & Sheng, G. (2016). A novel adsorbent TEMPO-mediated oxidized cellulose nanofibrils modified with PEI: Preparation, characterization, and application for Cu (II) removal. *Journal of Hazardous Materials, 316*, 11–18.
Zhang, Y., Guan, J., Wang, X., Yu, J., & Ding, B. (2017). Balsam-pear-skin-Like porous polyacrylonitrile nanofibrous membranes grafted with polyethyleneimine for post-combustion CO_2 capture. *ACS Applied Materials & Interfaces, 9*, 41087–41098.